Time-resolved spatial profile of TEA CO_2 laser pulses: influence of the gas mixture and intracavity apertures

Fernando Encinas-Sanz, Julio Serna, Rosario Martínez-Herrero, and Pedro M. Mejías

Departamento de Óptica, Facultad de Ciencias Físicas, Universidad Complutense, 28040 Madrid, Spain

Received November 8, 2000; revised manuscript received January 16, 2001; accepted January 22, 2001

The evolution of the intensity profile of transversely excited atmospheric CO_2 laser pulses is investigated within the intensity moment formalism. The beam quality factor M^2 is used to study the mode evolution. Attention is focused on the influence of both the gas mixture (N_2:CO_2:He) and the diameter of an intracavity diaphragm placed to attenuate higher-order modes. The degree of accuracy that can be attained by approximating the laser field amplitude by means of the lower-order terms of a Hermite–Gauss expansion is also analyzed. In particular, a bound for the truncation error is given in terms of two time-resolved spatial parameters, namely the beam width and the M^2 parameter. © 2001 Optical Society of America

OCIS codes: 140.3460, 140.3470.

1. INTRODUCTION

In the past decade, increasing efforts have been devoted to characterizing the spatial behavior of light fields. The transversal structure of a beam has been represented by means of merit figures and overall parameters. Among the different proposals, the description based on the so-called intensity moments of the beam[1–6] appears at present to be the most satisfactory one, and it has been adopted to rigorously define a number of International Organization for Standardization standards for continuous-wave beams.[7]

However, the time-varying aspects of transversal profiles of laser pulses have been considered in only a few papers in recent years.[8–12] More specifically, the evolution of the spatial profile of transversely excited atmospheric (TEA) CO_2 laser pulses along the pulse duration was recently investigated[13,14] within the so-called intensity-moment formalism. Attention was concentrated on the time evolution of the transversal modes in the laser cavity. More specifically, the studies were concerned mainly with both the instant at which the presence of a particular mode begins to be significant and the time interval during which such a pulse grows to reach a quasi-stationary intensity profile. In this connection, the time-varying beam-quality factor M^2 has been revealed to be a useful tool in investigating the mode evolution.[14]

In the present paper we proceed further with this research. Thus after describing in Section 2 the experimental setup used in the measurements, in Section 3 we investigate, for the pulses emitted by TEA CO_2 laser devices, the influence of the gas mixture (N_2:CO_2:He) as well as the dependence on the size of an intracavity diaphragm used to attenuate higher-order modes. In Section 4 the degree of accuracy that can be reached by approximating the instantaneous laser field by means of lower-order terms of a Hermite–Gauss expansion is evaluated as a function of two time-resolved spatial parameters, namely, the beam width (at the waist plane) and the beam-quality factor M^2 (demonstrations are given in Appendix A). Finally, the main results are summarized in the concluding Section 5.

2. EXPERIMENTAL SETUP AND BASIC DEFINITIONS

The laser device and the experimental arrangement used for the measurements (see Fig. 1) have been detailed elsewhere,[14] so here we will limit ourselves to a short description.

The laser resonator is half-symmetric, with a curved mirror (radius of curvature 10 m) and a flat output mirror separated 1120 mm. A Brewster plate is placed inside the cavity to get a linearly polarized beam. To study the evolution of the beam parameters, we create time slices of 10 ns (much shorter than the complete pulse duration of approximately 2–3 μs) by means of an electro-optical switching device based on a CdTe crystal and a polarizer. The slice width is controlled by the length of the coaxial forming cable that connects a spark gap with the high-voltage charge resistor. The spark gap is used to trigger the system by collecting some deflected light from the polarizer. The relative position of the time slice within the laser pulse is defined by the length of the delay cable between the spark gap and the switching device. Finally, the ensemble pyroelectric camera (Spiricon PYROCAM I), the laser beam analyzer, and the computer measure the beam width averaged during each time slice, i.e.,

$$\langle x^2\rangle(z_0, t_0) = \frac{1}{H_{t_0}} \int_{t_0}^{t_0+\Delta t} \mathrm{d}t \int\int x^2 |f|^2 \mathrm{d}x\mathrm{d}y, \qquad (1)$$

where f denotes the field amplitude at plane z_0, $\Delta t \simeq 10$ ns represents the FWHM temporal thickness of the time slice at time t_0, and

0740-3232/2001/071734-07$15.00

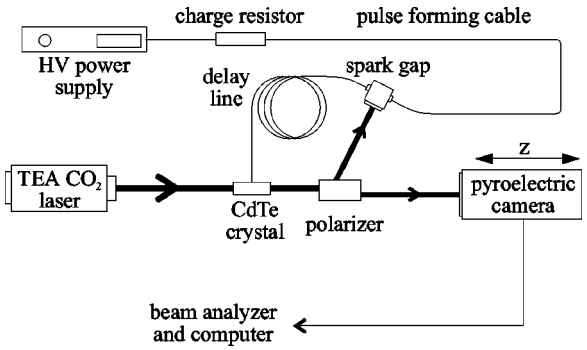

Fig. 1. Experimental setup (simplified) used to measure the time-resolved M^2 factor.

$$H_{t_0} = \int_{t_0}^{t_0+\Delta t} \mathrm{d}t \int\int |f|^2 \mathrm{d}x\,\mathrm{d}y \tag{2}$$

is the total energy of the time slice. Within the paraxial approach, the behavior of $\langle x^2 \rangle$ is quadratic with distance and can be expressed in terms of the second-order intensity moments $\langle x^2 \rangle$, $\langle x\,\theta \rangle$, and $\langle \theta^2 \rangle$ at some initial plane.[3,6] $\langle \theta^2 \rangle$ represents the far-field divergence associated with the x variable (again averaged over Δt), and $\langle x\,\theta \rangle$ denotes the crossed moment that gives the position of the waist plane from condition $\langle x\,\theta \rangle = 0$. These three second-order moments are measurable quantities and can be obtained from the experimental data.

As was pointed out in a previous paper,[14] pulse evolution can be inferred from the determination of the time-resolved beam-quality factor M^2, which, in the bidimensional case, is defined as

$$M^2(t_0) = (4k^2 \langle x^2 \rangle_w \langle \theta^2 \rangle)^{1/2}, \tag{3}$$

where $k = 2\pi/\lambda$ ($\lambda = 10.6\,\mu$m) is the wave number of the light and subscript w refers to the beam waist plane, in which the product $\langle x^2 \rangle \langle \theta^2 \rangle$ reaches an absolute minimum. For convenience and without loss of generality, it has been assumed that the first-order intensity moments are zero.

3. EXPERIMENTAL RESULTS

Using the above arrangement, we report in this section the experimental results concerning the evolution of the transversal structure of the pulse when either the size of an intracavity circular diaphragm or the gas mixture are varied. In all cases, for each time slice the values of $\langle x^2 \rangle$ measured versus propagation distance z_0 are fitted to a parabolic curve (which is the expected analytical behavior within the paraxial approach). The value of M^2 is then obtained from the parameters that define the fitting parabola.

A. Dependence on the Size of the Adjustable Intracavity Aperture

To show this dependence, we have represented in Fig. 2 the evolution of the M^2 factor along the pulse length for three intracavity diaphragms whose diameters are d = 9, 10, and 11 mm. In all of the measurements the gas mixture was N_2:CO_2:He = 2:1:5.4. Let us analyze each case separately.

1. d = 9 mm. In this case the transversal structure of the pulse is nearly Gaussian, and no actual evolution occurs. The intensity profile remains constant along the pulse [see Fig. 3(a)].

2. d = 10 mm. There is now only one mode at the leading edge of the pulse ($t_0 \lesssim 100$ ns), and its spatial structure is almost Gaussian. It should be noted that in the present work, we associate the term "modes" with definite spatial structures of the laser field within the loaded resonator. The existence of different modes would then indicate the presence of different transversal-mode resonance frequencies, as confirmed from the mode beating generated by heterodyne interference experiments. In the transition interval ($100 \lesssim t_0 \lesssim 500$ ns), the M^2 factor increases smoothly, a second mode grows, and the transversal profile of any time slice is no longer Gaussian. Finally, at the rear edge of the pulse ($t_0 \gtrsim 500$ ns), the beam profile exhibits a depleted-center intensity structure [see Fig. 3(b)], which is maintained nearly constant during the rest of the pulse.

3. d = 11 mm. In this case only two regions can be clearly observed in the s-shaped curve for the M^2 parameter: As soon as the pulse begins to be detected, two modes begin to grow, competing with each other, and the quasi-stationary spatial behavior is reached at $t_0 \sim 400$ ns. The intensity profile shows a nearly doughnut-shaped structure [see Fig. 3(c)].

We want to emphasize the critical influence of diffraction in the spatial structure formation for values of the diaphragm diameter higher than 9 mm.

The above three cases summarize the different types of evolution that can be observed in this kind of pulse: For values of d lower than 9 mm, the beam-quality factor, and consequently the transversal profile of the pulse, remains

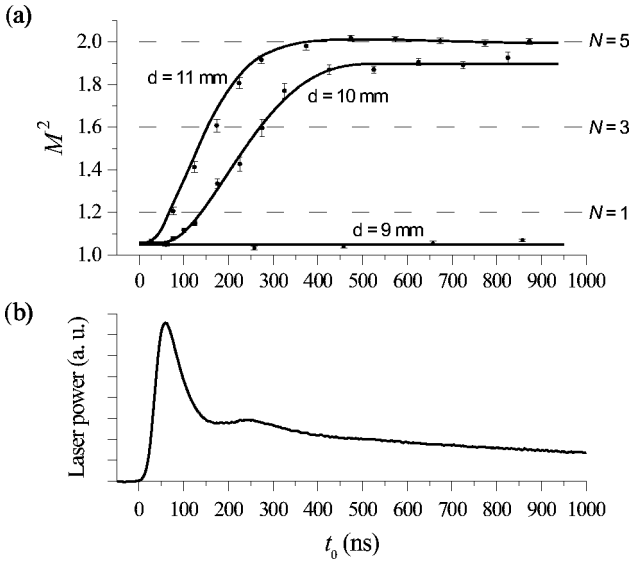

Fig. 2. (a) Evolution of the beam-quality factor along the pulse duration for three values of the diameter d of the intracavity aperture. Gas mixture was N_2:CO_2:He = 2:1:5.4. The values of N refer to the highest order of the Hermite–Gauss functions that we need to combine to approximate the transversal field whose M^2 factor lies under the corresponding dashed horizontal line with a relative error lower than 10% (see Section 4). (b) Pulse power (in arbitrary units) plotted for time reference.

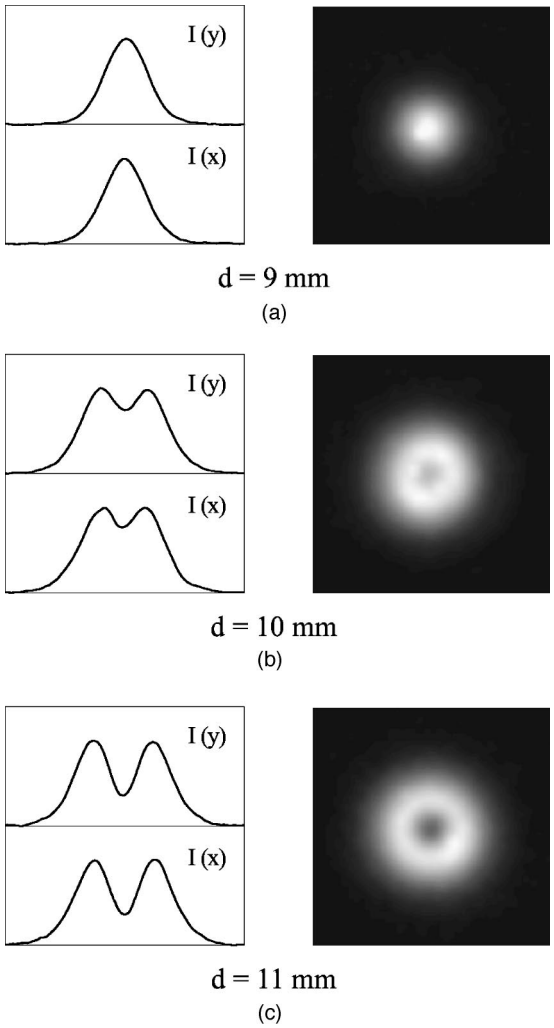

Fig. 3. Intensity profiles at $t_0 = 850$ ns for three intracavity diaphragms. The right-hand side of this figure shows the front-view intensity distributions.

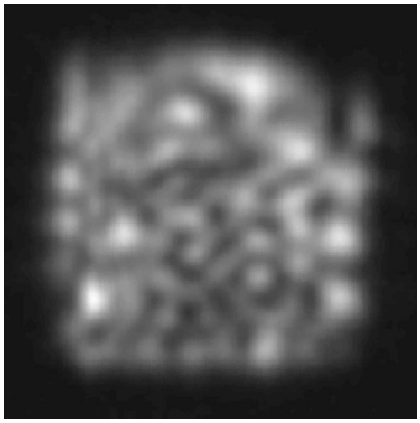

Fig. 4. Typical front-view intensity distribution of any time slice when no intracavity diaphragm is placed inside the laser cavity. The figure exhibits a chaotic spatial behavior.

constant. In contrast, for d higher than 11 mm, the M^2 parameter begins to deteriorate from the beginning of the pulse. In the limit case where no intracavity diaphragm is placed inside the laser cavity, the transversal profile of any time slice shows the chaotic spatial behavior plotted in Fig. 4. This behavior is due to the presence of an exceedingly high number of transversal modes caused by the significant reduction of the boundary diffraction.

B. Influence of the Gas Mixture

In Fig. 5 the evolution of the intensity profile for two gas mixtures, namely, N_2:CO_2:He = 2:1:5.4 [Fig. 5(a)] and N_2:CO_2:He = 2:0.6:5.4 [Fig. 5(b)] is compared. Diaphragm diameter was $d = 11$ mm. The behavior of the time-resolved M^2 parameter in both cases is plotted in Fig. 6. As is quite apparent from this figure, a higher presence of CO_2 increases the laser output power, but the cost to be paid is a faster beam-quality degradation. Furthermore, we see that higher-order modes begin to grow even during the gain-switch peak of the pulse. In contrast, when the CO_2 concentration decreases in the gas mixture, higher-order modes require supplementary time to grow. It could be said that the appearance of such modes is delayed with respect to the former case. In fact, the transversal profile of the time slices remains nearly Gaussian at the leading edge of the pulse ($t_0 \lesssim 200$ ns). In this case, Fig. 6 also reveals that higher-order modes begin to be significant after the complete gain-switch peak.

It is important to note that the time origin of the curves plotted in Fig. 6 has been chosen as the moment when the pulses are strong enough to be detected by the photon-drag detector over the noise level. Figure 7 shows that with respect to the instant that the pumping discharge begins (which can be considered as the absolute time reference), the cavity takes more time to start lasing when the presence of CO_2 decreases, as expected. In the present case, the delay approaches 200 ns.

4. TRUNCATION ERROR IN THE HERMITE–GAUSS EXPANSION OF THE TIME-RESOLVED LASER AMPLITUDE

As is well known, the laser beam amplitude can be expressed formally as a superposition of Hermite–Gauss functions. At the waist plane, we can write

$$f(x, y, t) = \sum_{n,m=0}^{\infty} c_{nm}(t) u_n(x) u_m(y), \tag{4}$$

where $f(x, y, t)$ represents the field amplitude, transversal to the propagation direction (z axis), associated with a fixed but arbitrary time slice; c_{nm} are constant coefficients (for each t); and u_p denotes the Hermite-Gauss functions,

$$u_p(\xi) = \beta_p H_p(\gamma\xi)\exp(-\gamma^2\xi^2/2), \qquad \xi = x, y, \tag{5}$$

where β_p is a constant, H_p is the Hermite polynomial of order p and γ is another constant, which will be specified later.

In general, an infinite number of terms of the series that appears in Eq. (4) is required to exactly fit the laser field $f(x, y, t)$. In practice, however, only a finite (and frequently small) number of Hermite–Gauss functions contribute in a significant way to the field amplitude. In the present section we will determine the highest order of the Hermite–Gauss functions that we need to compute in order to reproduce the exact (but, *a priori*, unknown) laser amplitude with a given accuracy. The results are

expressed in terms of measurable spatial parameters of the beam and will be applied to the pulses considered in Section 3.

Let us then approach the exact field $f(x, y, t)$ by means of the approximate field $f_N(x, y, t)$ given by

$$f_N(x, y, t) = \sum_{n,m=0}^{N} c_{nm}(t) u_n(x) u_m(y). \tag{6}$$

The truncation of the infinite series that gives the exact field involves a relative error ϵ defined as follows:

$$\epsilon(t_0) = \frac{\int_{t_0}^{t_0+\Delta t} \mathrm{d}t \int\int |f - f_N|^2 \mathrm{d}x\mathrm{d}y}{\int_{t_0}^{t_0+\Delta t} \mathrm{d}t \int\int |f|^2 \mathrm{d}x\mathrm{d}y}, \tag{7}$$

where Δt is the temporal width of the time slice (at t_0) that we have chosen. The value of ϵ can be regarded as the (overall) degree of accuracy of the approach. It will be useful to introduce the following coefficients:

$$C_{ab}^{cd}(t_0) = \int_{t_0}^{t_0+\Delta t} c_{ab}^{\star}(t) c_{cd}(t) \mathrm{d}t. \tag{8}$$

In terms of such coefficients we have

$$\int_{t_0}^{t_0+\Delta t} \mathrm{d}t \int\int |f - f_N|^2 \mathrm{d}x\mathrm{d}y = \sum_{n,m=N+1}^{\infty} C_{nm}^{nm}(t_0), \tag{9}$$

$$\int_{t_0}^{t_0+\Delta t} \mathrm{d}t \int\int |f|^2 \mathrm{d}x\mathrm{d}y = \sum_{n,m=0}^{\infty} C_{nm}^{nm}(t_0). \tag{10}$$

Taking this into account, the truncation error $\epsilon(t_0)$ becomes

$$\epsilon(t_0) = \sum_{n,m=N+1}^{\infty} C_{nm}^{nm}(t_0), \tag{11}$$

where $\mathcal{C}_{ab}^{cd}$ are the normalized C_{ab}^{cd}, i.e.,

$$\mathcal{C}_{ab}^{cd} = \frac{C_{ab}^{cd}(t_0)}{\sum_{n,m=0}^{\infty} C_{nm}^{nm}(t_0)}. \tag{12}$$

Let us now assume, for the sake of simplicity, that the values of the (time-resolved) beam size at the waist, $\langle x^2 \rangle_w$, and of the bidimensional beam-quality factor M^2 associated with the Cartesian transversal axes x and y

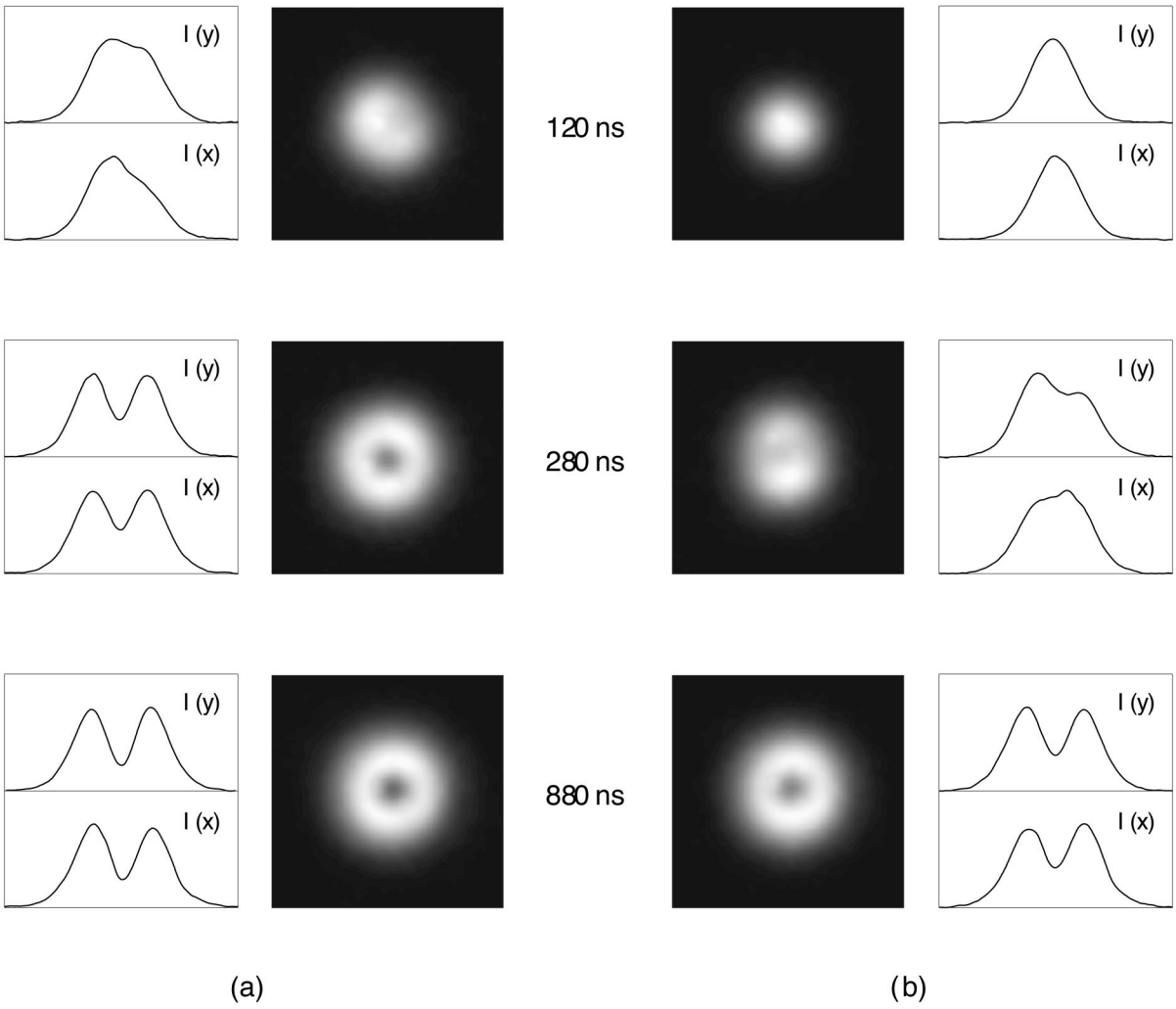

Fig. 5. Evolution of the intensity profile for two gas mixtures. (a) N_2:CO_2:He = 2:1:5.4 and (b) N_2:CO_2:He = 2:0.6:5.4. Diaphragm diameter was $d = 11$ mm. The temporal position of each time slice is indicated in the figure.

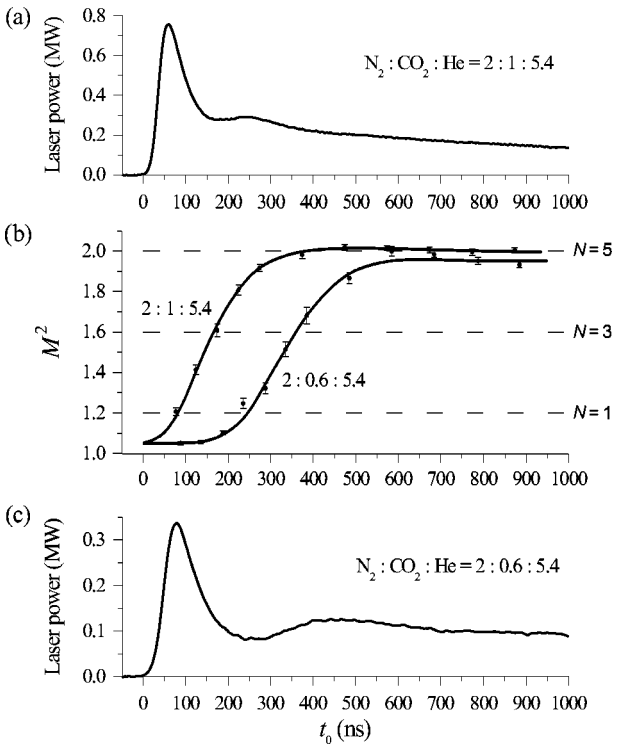

Fig. 6. Evolution of the M^2 factor along the pulse duration for two gas mixtures. As in Fig. 2, N refers to those regions of the curve whose M^2 factor lies under the corresponding horizontal line. Diaphragm diameter was $d = 11$ mm. In (a) and (c) the pulse power associated with each gas mixture is plotted for time reference.

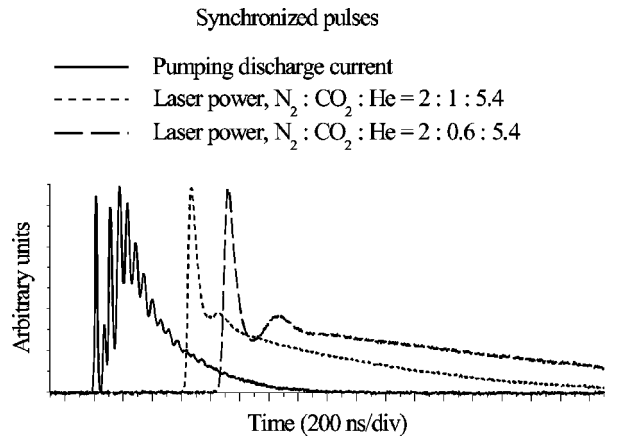

Fig. 7. Evolution of the power (in arbitrary units) of the synchronized pulses (dotted and dashed curves) for two gas mixtures. The current of the pumping discharge is also plotted (solid curve) for time reference.

are the same (generalization to an arbitrary case is straightforward). It is then shown in Appendix A that the relative error $\epsilon(t_0)$ fulfills

$$\epsilon \leqslant \frac{1}{4N}\frac{(M^2)^2 + s^2 - 2s}{s}, \tag{13}$$

where

$$s = 2\gamma^2\langle x^2\rangle_w . \tag{14}$$

Relation (13) establishes, in a quantitative way, a bound for the truncation error in terms of measurable spatial parameters. Note that the values of $\langle x^2\rangle_w$ and M^2 depend on the time slice that we are considering. Accordingly, for a fixed ϵ, the value of N would also depend on the selected time slice.

On the other hand, the constant γ that appears in Eq. (14) has not yet been fixed. Frequently γ is inferred from the geometry of the empty cavity and remains constant along the pulse duration. However, this is not the only possible choice. In fact, it is also shown in Appendix A that the truncation error is minimized by choosing γ to be that of the so-called embedded Gaussian beam[4,15,16] associated to the field f at time t_0. In other words, the value of $\gamma_{\min}$ that minimizes the truncation error reads

$$\gamma_{\min}^2 = \frac{M^2}{2\langle x^2\rangle_w}, \tag{15}$$

where $\gamma_{\min}$ is now a function of time. Relation (13) then becomes

$$\epsilon \leqslant \frac{1}{2N}(M^2 - 1), \tag{16}$$

which closely resembles the expression obtained for a Laguerre–Gauss expansion of axially symmetric beams.[17] Some important differences should, however, be noted with respect to the Laguerre–Gauss case. In that case, the calculations apply for continuous-wave laser beams, so that ϵ, N, and M are time invariant. Furthermore, the value of N is directly associated with the number of terms, $N + 1$, of the Laguerre–Gauss series. In the present paper, however, for a fixed value of the truncation error, the parameter M^2 and, consequently, N, depend on time. Moreover, N provides the highest order of the Hermite–Gauss functions that we should combine to approach the transversal field at each time slice with the prescribed overall accuracy. Accordingly, if, for example, $N = 1$, the truncated Hermite–Gauss series would contain four terms, namely, $u_0(x)u_0(y)$, $u_0(x)u_1(y)$, $u_1(x)u_0(y)$, and $u_1(x)u_1(y)$, whereas the finite Laguerre–Gauss expansion would handle only two terms, associated with the Laguerre–Gauss polynomials $L_0{}^0$ and $L_1{}^0$.

As a general consequence from relation (16), it follows immediately that for a fixed ϵ, N must increase as the beam quality deteriorates (M^2 increase).

Concerning the pulses that we have considered in the present work, the application of relation (16) is synthesized by the dashed horizontal lines of Figs. 2 and 6, where we have considered $\epsilon(t_0) < 10\%$ in all the cases. The respective values of N refer to those regions of the pulse evolution whose beam-quality factor lies under the corresponding horizontal line. In particular, $N = 1$ when the diameter of the intracavity diaphragm is lower than 9 mm (for a truncation error lower than 5%). To obtain the same accuracy at the leading edge of the pulses when $M^2 < 1.2$ (for the apertures and the gas mixtures that we have analyzed), we would need $N = 2$. Finally, at the rear edge of the pulses where $M^2 \sim 2$, we have to consider $N = 5$ for a relative error ϵ lower than 10%.

5. CONCLUSIONS

The second-order intensity moments have been shown to be useful in analyzing the growing process and evolution of the modes for the pulses emitted by TEA CO_2 laser devices. In particular, from the measurement of the time-resolved M^2 factor, it can be concluded that

1. The influence of diffraction on the evolution of the transversal spatial structure of the pulse exhibits a critical behavior when the diameter of the intracavity diaphragm closely approaches a certain value ($d = 9$ mm).
2. Higher-order modes require supplementary time to grow as long as diffraction losses increase (d decreases). In the lower limit ($d \to 0$) only the fundamental mode would appear. On the other hand, if no diaphragm is placed inside the cavity (high Fresnel number case), the pulse exhibits a chaotic spatial structure at any point in time.
3. A higher concentration of CO_2 in the gas mixture (higher laser output power) generates a faster beam-quality degradation, owing to the fact that higher-order modes begin to grow from the beginning of the pulse.
4. The highest order of the Hermite–Gauss functions that contribute significantly to the time-resolved laser amplitude can be determined in a simple way. The truncated Hermite–Gauss series could then be used as a suitable trial function to reduce time-consuming computations, such as those required to numerically solve the Maxwell–Bloch equations governing the dynamics of the laser emission.[18] This problem deserves further study.

APPENDIX A

To demonstrate relation (13) let us first remark that at each time slice defined by t_0 the second-order intensity moments (in the x variable) of the laser field $f(x, y, t)$ are the same as those of a field whose correlation function is

$$\Gamma(x_1, x_2, t_0) = \int_{t_0}^{t_0+\Delta t} \mathrm{d}t \int f^*(x_1, y, t) f(x_2, y, t) \mathrm{d}y, \tag{A1}$$

$$= \sum_{n,m=0}^{\infty} R_{nm}(t_0) u_n(x_1) u_m(x_2), \tag{A2}$$

where

$$R_{nm}(t_0) = \sum_{b=0}^{\infty} C_{nb}^{mb}(t_0). \tag{A3}$$

Taking this into account as well as the recurrence properties of the Hermite–Gauss functions and their derivatives,[19] it can be shown in a way similar to that used in Ref. 20 that the following relations hold for the laser amplitude f:

$$2\gamma^2\langle x^2\rangle = \sum_{n=0}^{\infty} \tilde{R}_{nn} + 2\sum_{n=0}^{\infty} [(n+2)(n+1)]^{1/2} \times \mathrm{Re}(\tilde{R}_{n,n+2}), \tag{A4}$$

$$(M_x^2)^2 = \left[\sum_{n=0}^{\infty} (2n+1)\tilde{R}_{nn}\right]^2 - 4\left|\sum_{n=0}^{\infty} [(n+2)(n+1)]^{1/2} \tilde{R}_{n,n+2}\right|^2, \tag{A5}$$

$$0 = \sum_{n=0}^{\infty} [(n+2)(n+1)]^{1/2} \mathrm{Im}(\tilde{R}_{n,n+2}), \tag{A6}$$

where

$$\tilde{R}_{nm}(t_0) = \sum_{b=0}^{\infty} C_{nb}^{mb}(t_0), \tag{A7}$$

and the subscript x in the M^2 factor indicates that we are considering the x axis. It should be noted that Eq. (A6) applies because we are considering the waist plane. From these equations we have

$$\sum_{n=0}^{\infty} (2n+1)\tilde{R}_{nn}(t_0) = \frac{(M_x^2)^2 + 4\gamma^4\langle x^2\rangle_w^2}{4\gamma^2\langle x^2\rangle_w}. \tag{A8}$$

If we now consider the intensity moments in the y variable and follow a procedure analogous to that used to get the above equation, we obtain

$$\sum_{m=0}^{\infty} (2m+1)\tilde{S}_{mm}(t_0) = \frac{(M_y^2)^2 + 4\gamma^4\langle y^2\rangle_w^2}{4\gamma^2\langle y^2\rangle_w}, \tag{A9}$$

where

$$\tilde{S}_{nm}(t_0) = \sum_{a=0}^{\infty} C_{an}^{am}(t_0), \tag{A10}$$

and the bidimensional M_y^2 factor is associated with the y variable. Let us now assume, for simplicity, that $\langle x^2\rangle_w = \langle y^2\rangle_w$ and $M_x^2 = M_y^2 = M^2$, as occurs frequently in practice (the results can be generalized to an arbitrary case in a straightforward way). Taking this into account, since

$$\sum_{n=0}^{\infty} \tilde{R}_{nn}(t_0) = \sum_{m=0}^{\infty} \tilde{S}_{mm}(t_0) = 1, \tag{A11}$$

we can write

$$\sum_{n=0}^{\infty} n\tilde{R}_{nn}(t_0) + \sum_{m=0}^{\infty} m\tilde{S}_{mm}(t_0) = \frac{(M^2)^2 + s^2 - 2s}{2s}, \tag{A12}$$

where

$$s = 2\gamma^2\langle x^2\rangle_w. \tag{A13}$$

Finally, since

$$\sum_{n,m=0}^{\infty} (n+m) C_{nm}^{nm}(t_0) \geqslant 2N \sum_{n,m=N+1}^{\infty} C_{nm}^{nm}(t_0), \tag{A14}$$

substitution in Eq. (A12) directly goes into relation (13); Q.E.D.

Let us now show that the value of γ that minimizes ϵ is given by Eq. (15). Starting from relation (13), the condition

$$\frac{\partial}{\partial s}\left[\frac{(M^2)^2 + s^2 - 2s}{2s}\right] = 0 \tag{A15}$$

implies

$$s_{\min} = M^2; \tag{A16}$$

that is,

$$\gamma_{\min}^2 = \frac{M^2}{2\langle x^2\rangle_w}, \tag{A17}$$

which corresponds to a minimum because

$$\frac{\partial^2}{\partial s^2}\left[\frac{(M^2)^2 + s^2 - 2s}{2s}\right]\Bigg|_{s_{\min}} = \frac{2}{s_{\min}} > 0; \quad \text{Q.E.D.} \tag{A18}$$

ACKNOWLEDGMENT

This work was supported by the Comisión Interministerial de Ciencia y Tecnología of Spain under project PB97-0295.

Corresponding author Fernando Encinas-Sanz can be reached at the address on the title page or by e-mail at fencinas@eucmax.sim.ucm.es.

REFERENCES AND NOTES

1. M. J. Bastiaans, "Wigner distribution function and its application to first-order optics," J. Opt. Soc. Am. **69**, 1710–1716 (1979).
2. S. Lavi, R. Prochaska, and E. Keren, "Generalized beam parameters and transformation laws for partially coherent light," Appl. Opt. **27**, 3696–3703 (1988).
3. R. Simon, N. Mukunda, and E. C. G. Sudarshan, "Partially coherent beams and a generalized ABCD law," Opt. Commun. **65**, 322–328 (1988).
4. A. E. Siegman, "New developments in laser resonators," in *Laser Resonators*, D. A. Holmes, ed., Proc. SPIE **1224**, 2–14 (1990).
5. J. Serna, R. Martínez-Herrero, and P. M. Mejías, "Parametric characterization of general partially coherent beams propagating through ABCD optical systems," J. Opt. Soc. Am. A **8**, 1094–1098 (1991).
6. H. Weber, "Propagation of higher-order intensity moments in quadratic-index media," Opt. Quantum Electron. **24**, 1027–1049 (1992).
7. ISO 11146:1999. "Lasers and laser-related equipment—Test methods for laser beam parameters—Beam widths, divergence angle and beam propagation factor," (International Organization for Standardization, Geneva, Switzerland).
8. A. Caprara and G. C. Reali, "Time-resolved M^2 of nanosecond pulses from a Q-switched variable-reflectivity-mirror Nd:YAG laser," Opt. Lett. **17**, 414–416 (1992).
9. T. Omatsu and K. Kuroda, "Time-resolved measurements of spatial coherence of a copper vapor laser using a reversal shearing interferometer," Opt. Commun. **87**, 278–286 (1992).
10. J. J. Chang, "Time-resolved beam-quality characterization of copper vapor lasers with unstable resonators," Appl. Opt. **33**, 2255–2265 (1994).
11. P. M. Mejías and R. Martínez-Herrero, "Time-resolved spatial parametric characterization of pulsed light beams," Opt. Lett. **20**, 660–662 (1995).
12. C. Palma, C. Panzera, M. R. Perrone, G. De Nunzio, and A. Mascello, "Parameters evolution of laser beams with quite general transverse intensity profile," IEEE J. Quantum Electron. **33**, 2178–2187 (1997).
13. C. Martínez, F. Encinas-Sanz, J. Serna, P. M. Mejías, and R. Martínez-Herrero, "On the parametric characterization of the transversal spatial structure of laser pulses," Opt. Commun. **139**, 299–305 (1997).
14. F. Encinas-Sanz, J. Serna, C. Martínez, R. Martínez-Herrero, and P. M. Mejías, "Time-varying beam quality factor and mode evolution in TEA CO_2 laser pulses," IEEE J. Quantum Electron. **34**, 1835–1838 (1998).
15. A. E. Siegman, "Defining the effective radius of curvature for a nonideal optical beam," IEEE J. Quantum Electron. **27**, 1146–1148 (1991).
16. R. Borghi, F. Gori, M. Santarsiero, and S. Vicalvi, "Shape-invariance error for some classes of coherent light beams," in *4th Workshop on Laser Beam and Optics Characterization*, A. Giesen and M. Morin, eds. (VDI-Technologiezentrum, Düsseldorf, 1997), p. 106–117.
17. P. M. Mejías and R. Martínez-Herrero, "Truncation error of the Laguerre–Gauss expansion of axially symmetric beams in terms of second-order intensity moments," Pure Appl. Opt. **7**, 1231–1236 (1998).
18. F. Encinas-Sanz, O. G. Calderón, R. Gutiérrez-Castrejón, and J. M. Guerra, "Measurement of the spatiotemporal dynamics of simple transverse patterns in a pulsed transversely excited atmospheric CO_2 laser," Phys. Rev. A **59**, 4764–4772 (1999).
19. I. S. Gradshteyn and I. M. Ryzhik, *Table of Integrals, Series and Products* (Academic, San Diego, Calif., 1980).
20. R. Martínez-Herrero and P. M. Mejías, "Expansion of the cross spectral density function of general fields and its application to beam characterization," Opt. Commun. **94**, 197–202 (1992).